Clim Dyn (2018) 50:3853–3864
DOI 10.1007/s00382-017-3850-3

Heat wave probability in the changing climate of the Southwest US

Kristen Guirguis[1] · Alexander Gershunov[1] · Daniel R. Cayan[1] · David W. Pierce[1]

Received: 28 November 2016 / Accepted: 1 August 2017 / Published online: 18 September 2017

Abstract Analyses of observed non-Gaussian daily minimum and maximum temperature probability distribution functions (PDFs) in the Southwest US highlight the importance of variance and warm tail length in determining future heat wave probability. Even if no PDF shape change occurs with climate change, locations with shorter warm tails and/or smaller variance will see a greater increase in heat wave probability, defined as exceedances above the historical 95th percentile threshold, than will long tailed/larger variance distributions. Projections from ten downscaled CMIP5 models show important geospatial differences in the amount of warming expected for a location. However, changes in heat wave probability do not directly follow changes in background warming. Projected changes in heat wave probability are largely explained by a rigid shift of the daily temperature distribution. In some locations where there is more warming, future heat wave probability is buffered somewhat by longer warm tails. In other parts of the Southwest where there is less warming, heat wave probability is relatively enhanced because of shorter tailed PDFs. Effects of PDF shape changes are generally small by comparison to those from a rigid shift, and fall within the range of uncertainty among models in the amount of warming expected by the end of the century.

Electronic supplementary material The online version of this article (doi:10.1007/s00382-017-3850-3) contains supplementary material, which is available to authorized users.

✉ Kristen Guirguis
kguirguis@ucsd.edu

[1] Scripps Institution of Oceanography, University of California, San Diego, 9500 Gilman Drive, Mail Code 0224, La Jolla, CA 92093, USA

1 Introduction

One of the most important challenges in preparing for global climate change is to understand future behavior of weather extremes at the local level. Temperature extremes in particular can stress resources and the economy via their effects on energy, health care demands and agriculture. Understanding the probability distribution of future temperatures including extremes has important implications for human and ecosystem acclimation. Global warming is expected to increase the probability of warm extremes while reducing the probability of cold extremes, as the temperature probability distribution function (PDF) shifts reflecting a warming mean climate. The behavior of this shift at the local level in terms of how daily weather statistics may change is not well understood.

It is recognized that changes in the temperature PDF due to anthropogenic climate change could have profound impacts on extreme temperature probabilities (IPCC 2012). Figure 1 provides an illustration of how climate change could affect warm temperature extremes depending on whether the PDF undergoes (a) a rigid shift, (b) a shift accompanied by a change in variance or (c) a shift accompanied by a change in symmetry. In all cases, the probability of hot weather is increased but by different amounts.

Changes to the summer temperature PDF can have important consequences for human health. Schar et al. (2004) demonstrated the role of increasing temperature variability in European summer heat waves in general and the unprecedented 2003 heat wave in particular, which was responsible for a staggering 15,000 deaths in France (Poumadere et al. 2005) and many more across Europe. Diffenbaugh et al. (2007) compared the 95th and 75th percentiles of minimum and maximum temperatures in the Mediterranean region and found preferential warming of the hot tail of the temperature PDF using a regional climate model forced by a

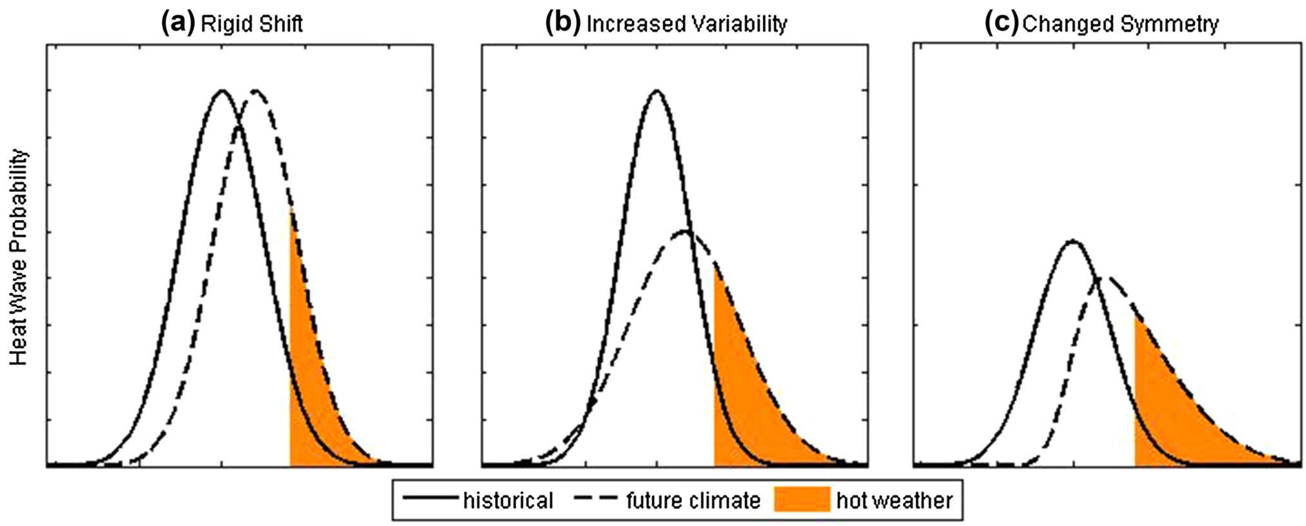

Fig. 1 Conceptual illustration showing possible changes in the temperature distribution due to climate change and the implications for future heat wave probability. In *all panels* the center of the distribution (mode) is shifted by 4 °C. **a** Shows a rigid shift in the distribution towards warmer temperatures with no change in shape or variance, **b** additionally undergoes an increase in variance, and **c** undergoes an increase in variance and the shape becomes positively skewed. This illustration is based on Figure SPM.3 of the IPPC Special Report on Extremes (IPCC 2012). The PDFs were modeled using the skew-normal probability distribution function

GCM under different greenhouse gas scenarios, which they attributed to surface moisture feedback mechanisms. Gershunov and Guirguis (2012) studied observed and projected heat wave activity over California and identified preferential coastal warming of the hot tail (95th percentile) relative to the median. Kodra and Ganguly (2014) explored changes in seasonal maxima (hottest day) and minima (coldest night) in CMIP5 projections using generalized extreme value (GEV) theory and found evidence that temperatures associated with the highest percentiles (e.g. the 95th) are projected to increase significantly more than those associated with the lowest (e.g. the 5th). Weaver et al. (2014) analyzed many realizations from the NCEP Climate Forecast System Version 2 over the 30-year period 1983–2012 and concluded that observed increases in temperature extremes globally and in the US are due to shifts in the mean temperature distribution and not from increasing temperature variability.

Extreme climate indices are often used to examine how climate change may be impacting society. Typically, these include measures of threshold exceedances such as days exceeding a specified temperature or percentile level (e.g. the Expert Team on Climate Change Detection and Indices, Zhang et al. 2011). A few studies have noted the nonlinear relationship between threshold exceedance probabilities and changes in the mean. Simolo et al. (2010, 2011) modeled this nonlinear relationship over Italy and Europe, respectively, to demonstrate the dominant role of the mean in explaining observed increases in warm temperature extremes. Ruff and Neelin (2012) demonstrated how the shape of the tail of the temperature PDF can dramatically impact the probability of extremes under global warming, showing that shifts-toward-warmer means of long tailed PDFs will exceed thresholds at a lower rate than shifts of near-Gaussian distributions. They recommended validating dynamical climate models in their representation of PDF tails if they are to be used to estimate changes in temperature extreme probabilities. Many studies have shown how surface or near-surface daily temperature distributions may depart from Gaussian (Ruff and Neelin 2012; Loikith et al. 2013; Perron and Sura 2013; Stefanova et al. 2013; Cavanaugh and Shen 2014; Guirguis et al. 2015). Therefore, while the examples in Fig. 1 and IPCC (2012) are useful for conceptualization, in practice we will likely see more complex changes due to geospatial differences in the native (historical) shape of the temperature PDF.

In this paper, we investigate implications of a changing climate on extreme temperature probabilities at a high spatial resolution over the geographically and climatically complex Southwest US. We consider the full PDF of daily maximum and minimum temperatures during summer (June–August) using observations and downscaled climate model projections from ten CMIP5 models. Following a discussion of data and methods, we describe the observed asymmetry in historical daily temperature PDFs and compare these with those from downscaled model projections (Sect. 4). We then summarize how the native shape of local PDFs results in geospatial differences in future extreme probability even under a uniform change in mean (Sect. 5) under which the distribution is shifted rigidly as in Fig. 1a but where the underlying distributions are not necessarily Gaussian. We then quantify effects of future changes in variability or symmetry of the temperature PDF in modifying the probability of extremes in future climate (Sect. 6), which represents changes of the type shown in Fig. 1b, c. A summary and discussion is provided in Sect. 7.

2 Data

2.1 Observed daily temperatures

We use daily maximum and minimum temperatures (Tmax and Tmin, respectively) from Livneh et al. (2013), which is a gridded product derived from daily station data interpolated to a 1/16° latitude–longitude grid (~6×6 km^2). The source data are the cooperative observer (coop) summaries of the day from the National Centers for Environmental Information (NCEI, formerly the National Climatic Data Center) supplemented by first-order Automated Surface Observing System observations (NCDC 2009). This product is an update/extension of the well-used product of Maurer et al. (2002), and is the training data set for the LOCA downscaling (described below) and so is the appropriate dataset for comparison with the 1/16° downscaled climate model projections. A comparison of the Livneh data with station observations is discussed in Guirguis et al. (2015). The study domain for this analysis is a large portion of the Southwest US (west of 100°W and south of 45°N).

2.2 CMIP5 models and LOCA downscaling

Ten GCMs previously evaluated as most suitable for regional climate assessment in California (California Department of Water Resources 2015) were chosen (ACCESS1-0, CanESM2, CCSM4, CESM1-BGC, CMCC-CMS, CNRM-CM5, GFDL-CM3, HadGEM2-CC, HadCEM2-ES, MIROC5) from the 32 models participating in the Coupled Model Intercomparison Project Phase 5 (CMIP5, Taylor et al. 2012) that had daily temperature and precipitation data available when this study was undertaken. Spatially coarse GCM information from the historical and RCP8.5 simulations was statistically downscaled onto a 1/16° grid using Localized Constructed Analogs (LOCA, Pierce et al. 2014) which included frequency dependent bias correction (Pierce et al. 2015).

LOCA is a constructed analog technique (van den Dool 1994) that begins by identifying the 30 observed days in the historical record that have the smallest RMS error between the observed day and the model day being downscaled. These 30 observed days are termed “analog days”. The 30 analog days are combined to construct a final result that is closer to the model day being downscaled than is any individual analog day. In earlier constructed analog approaches, the construction has been done by a weighted average of the 30 analog days over the entire domain being downscaled (e.g., Hidalgo et al. 2008), with the weights chosen to minimize the domain-wide error between the weighted sum and the model day being downscaled. However this averaging leads to a number of drawbacks as described in Pierce et al. (2014), including the reduction of extremes, increase in drizzle when downscaling precipitation, and sensitivity of the result to the spatial extent of the domain being downscaled. The LOCA technique instead uses a multi-scale spatial matching approach, without averaging, to construct the final analog day. From the initial pool of 30 analog days that best match the model day being downscaled over the wider region, the one single best matching day is selected that minimizes the RMS error between the observations and model day being downscaled in a $1° \times 1°$ box around the grid cell being downscaled. Since LOCA avoids the weighting averaging of the analog days, the overall averaging needed to construct the final field is greatly reduced, eliminating problems of over smoothing and providing better estimates of extremes and a more realistic spatial structure. For additional details see Pierce et al. (2014).

The bias correction method is based on the equidistant CDF matching method (EDCDFm; Li et al. 2010). Over the historical period EDCDFm devolves to ordinary Quantile Mapping (QM), so that downscaled model data in the historical period has nearly the same CDF as the Livneh training data set. For future periods, EDCDFm is designed to additively preserve changes in the shape of the PDF, by quantile, that may be projected by the GCMs to occur due to anthropogenic climate change. The results are then further bias adjusted to decrease errors in the representation of variance with frequency (Pierce et al. 2015).

3 Methods

The summer (June–August) temperature PDFs are modeled using the skew-normal (SN) PDF. The SN distribution is a theoretical probability distribution function that is specified by three parameters: location, scale and shape where location is a measure of central tendency, scale is a measure of dispersion about the central tendency, and shape is a measure of skew. These parameters are closely related to but not equal to the three first moments: mean, variance, and skewness, respectively. In particular, location is most closely aligned with the mode—much more a measure of central tendency than the mean, which can be unduly influenced by extremes, especially for skewed PDFs. Guirguis et al. (2015) used the SN to model daily winter temperature variability in the Southwest US and found it to be superior to Gaussian distributions in representing temperature PDFs in that region, including the tails. This result is similarly valid in summer (not shown).

Simolo et al. (2010, 2011) used the SN to effectively model the nonlinear relationship between extremes and the central tendency over Italy and Europe. The PDFs in Fig. 1 were modeled by varying the parameters of the SN PDF, illustrating the flexibility of the SN model. An advantage of the SN approach is the ability to estimate many different metrics from only three parameters. In this study, the SN approach is used to investigate effects on heat wave probability in future climate arising from a rigid shift and also from changes in scale or shape of daily temperature distributions.

The SN PDF of a continuous variable X can be represented using the standard normal density function ϕ and standard normal cumulative distribution Φ with an added shape parameter λ, as follows:

$$f(x) = 2\phi(x)\Phi(\lambda x), \quad \phi(x) = \exp\left(\frac{-x^2}{2}\right) \Big/ \sqrt{2\pi}, \quad \Phi(\lambda x) = \int_{-\infty}^{\lambda x} \phi(t)dt \tag{1}$$

Here, the distribution can be positively ($\lambda > 0$) or negatively ($\lambda < 0$) skewed, or can revert to the standard normal distribution in the case that $\lambda = 0$. We can make the transformation $Y = \xi + \omega x$ to include a location and scale parameter in Eq. (1), which is then said to have a SN distribution with parameters ξ, ω, and λ corresponding location, scale, and shape, respectively. The mean and variance are related to the SN parameters by

$$E\{Y\} = \xi + \omega\sqrt{2/\pi}\delta$$

$$\mathrm{var}\{Y\} = \omega^2\left(1 - 2\delta^2/\pi\right)$$

where $\delta = \lambda \Big/ \sqrt{1 + \lambda^2}$ (Azzalini and Capitanio 1999; Azzalini 2005a, b).

We fit SN PDFs to daily summer Tmax and Tmin. The SN fit was done first for the historical climate period 1961–1990 from Livneh data and from the ten downscaled CMIP5 models, and then for the end of the twenty-first century (2070–2099) from the ten downscaled model projections. The CMIP5 climate change projections were run under the RCP8.5 "business as usual" greenhouse gas emissions scenario. Recall that ξ, ω, and λ represent the location, scale, and shape parameters, respectively. Then the PDF for the historical period (H) and for future climate (F) can be represented by $PDF_H = f(\xi_H, \omega_H, \lambda_H)$ and $PDF_F = f(\xi_F, \omega_F, \lambda_F)$, respectively. In each case the parameters were estimated with maximum likelihood estimation using the R package 'sn' (Azzalini 2014). A hypothetical rigid shift outcome (S) preserves the historical scale and shape parameters, but shifts the location parameter by ΔT, or $PDF_S = f(\xi_H + \Delta T, \omega_H, \lambda_H)$.

Temperatures exceeding the historical 95th percentile are defined as heat waves in this study. In the historical period, heat wave probability is 5% by definition. In future climate, following convention, heat wave probability (hereinafter HWP) is defined as the proportion of days exceeding the historical 95th percentile threshold. In future climate projections, HWP can be calculated directly from the daily LOCA data, or from the cumulative distribution function (CDF) using the fitted SN parameters. We found little difference in the two methods, signifying a generally good fit of the SN model. For the "rigid shift" calculations HWP is calculated from the SN CDF using shape and scale parameters from the historical distribution.

4 Asymmetry of temperature distributions

Due to the complex topography in the Southwest, local climate can vary dramatically over relatively short geographic distances. Figure 2 displays the first three statistical moments of the summer temperature PDF for Tmax and Tmin, along with the warm tail length, which is calculated as the temperature difference between the 95th percentile and the mode. Tmax shows a north–south gradient in variance with stronger variance in the north and lesser variance in the south. The strongest negative skew (meaning longer cold tails and shorter warm tails) is seen over the Rocky Mountains and intermountain region, only slightly negative skewness is seen over southern Arizona and New Mexico, and positive skewness (meaning longer warm tails and shorter cold tails) is found over coastal California. The summer Tmin distribution shows less variance overall as compared with Tmax. Spatially, there is stronger variance over the intermountain region than at the California coast or locations that experience maritime influence from the Gulf of Mexico. The Tmin distribution shows a northwest–southeast gradient in skew with strong negative skew in the southeast and positive skew in the northwest. From Fig. 1d, h, warm tail length is strongly related to skew, accentuating the coast where heat waves are extraordinarily hot compared to typical temperatures, population density is high, and public health is inordinately vulnerable to heat (Guirguis et al. 2014).

Figure S1 shows the 10-model average of the first three moments and tail length. Due to the bias correction and downscaling methodology (Pierce et al. 2014), the modeled temperature PDFs appear similar to those observed. For Tmax, the spatial correlation (RMSE) with observations is 1.0 (0.93), 0.99 (0.13), 0.96 (0.10), and 0.94 (0.40) for mean, standard deviation, skewness, and tail length, respectively. For Tmin, these measures are 1.0 (0.97), 0.95 (0.15), 0.83 (0.16), and 0.87 (0.57), respectively. For Tmax,

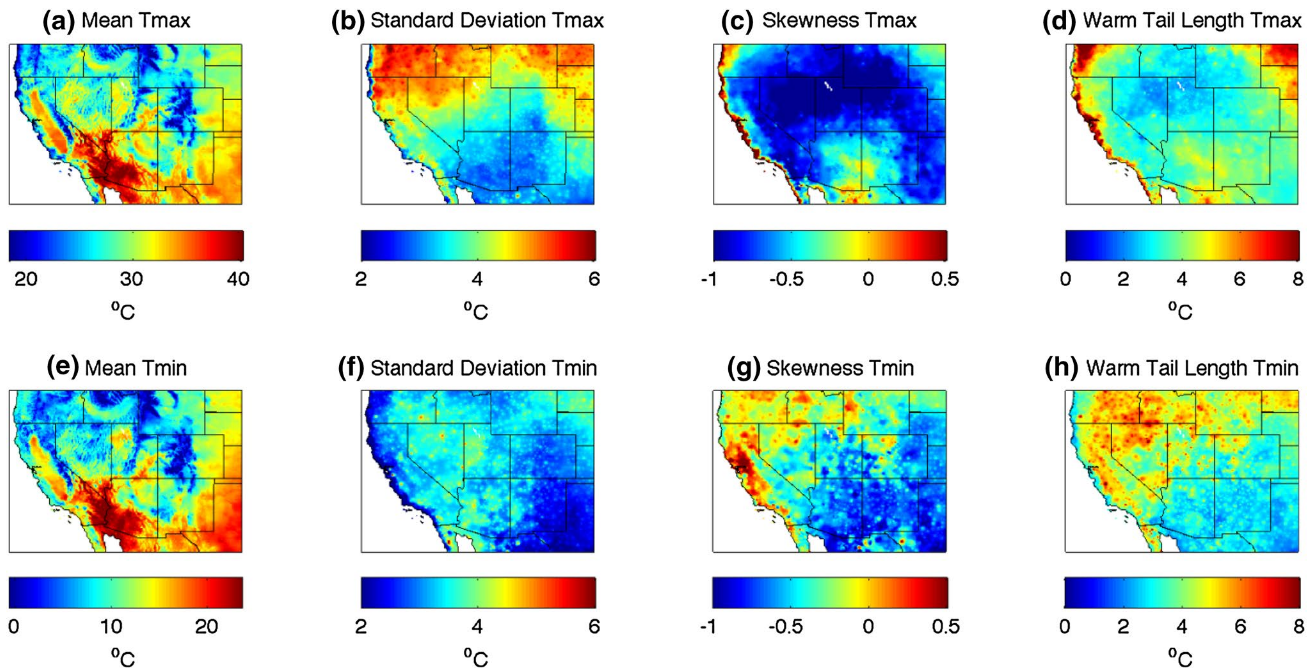

Fig. 2 First three statistical moments and warm tail length for JJA Tmax (**a**–**d**) and Tmin (**e**–**h**) according to Livneh observational data. Warm tail length is calculated as the temperature difference between the 95th percentile and the mode of the PDF

the downscaled ensemble is nearly indistinguishable from observations. For Tmin, there is a modest difference seen in skew, which ultimately affects measures of tail length. The LOCA methodology calculates Tmin as the residual between Tmax and diurnal temperature range, which likely explains the slight differences between observations and Tmin. Not surprisingly given the bias correction, the downscaled models represent the historical temperature PDFs very well.

5 Probability of extremes under a shifted mode assumption: effects of tail length and variance

First we explore geospatial differences in the probability of extremes that occur under the assumption of a rigid shift, where the scale and shape of the temperature PDF are held constant and future climate is represented by a uniform shift in the mode of the PDF. The uniform shifted mode means that at each location the historical PDF is shifted by a fixed ΔT. Geospatial differences in the probability of extremes are therefore due to geospatial differences in the shape of the historical daily temperature PDF across the region. In this experiment we shift all PDFs by 4 °C, which is less than the average summer change (5.9 °C) projected by the end of century over the domain under RCP8.5 according to the 10 downscaled models (note that projected temperature increases over land are higher than the more commonly quoted global averages, and summer warming is projected to be greater than annually averaged warming in this region). Figure 3a, b show the HWP resulting from a hypothetical uniform shift for Tmax and Tmin, respectively, and the difference is given in Fig. 3c. While historically HWP is 5% by definition, the uniform shift results in dramatic geospatial differences in HWP. Tmax HWP increases are small in some regions, such as coastal California, where values change from the historical value of 5% to only 6%. But other locations show a dramatic increase in HWP to more than 70%, with the highest resulting HWP values centered over the Great Basin and including parts of California and Texas where historical PDFs exhibit large negative skewness. For Tmin, we see HWP increase to reach probabilities in the range of 16–90%, with the highest probabilities in the Gulf region and coastal California. The geospatial pattern of HWP is related to geospatial differences in warm tail length and variance. For both Tmax and Tmin, variance is most strongly associated with HWP. The spatial correlation between HWP and variance is −0.69 and −0.82, for Tmax and Tmin, respectively. For warm tail length these correlations are −0.45 and −0.59, respectively. Warm tail length is strongly related to skew (r = 0.86 and 0.87 for Tmax and Tmin, respectively), and only weakly correlated with variance (r = −0.21 and 0.14 for Tmax and Tmin, respectively). We focus on warm tail length rather than skewness because we are focused on heat waves and therefore are interested in isolating the right hand side of

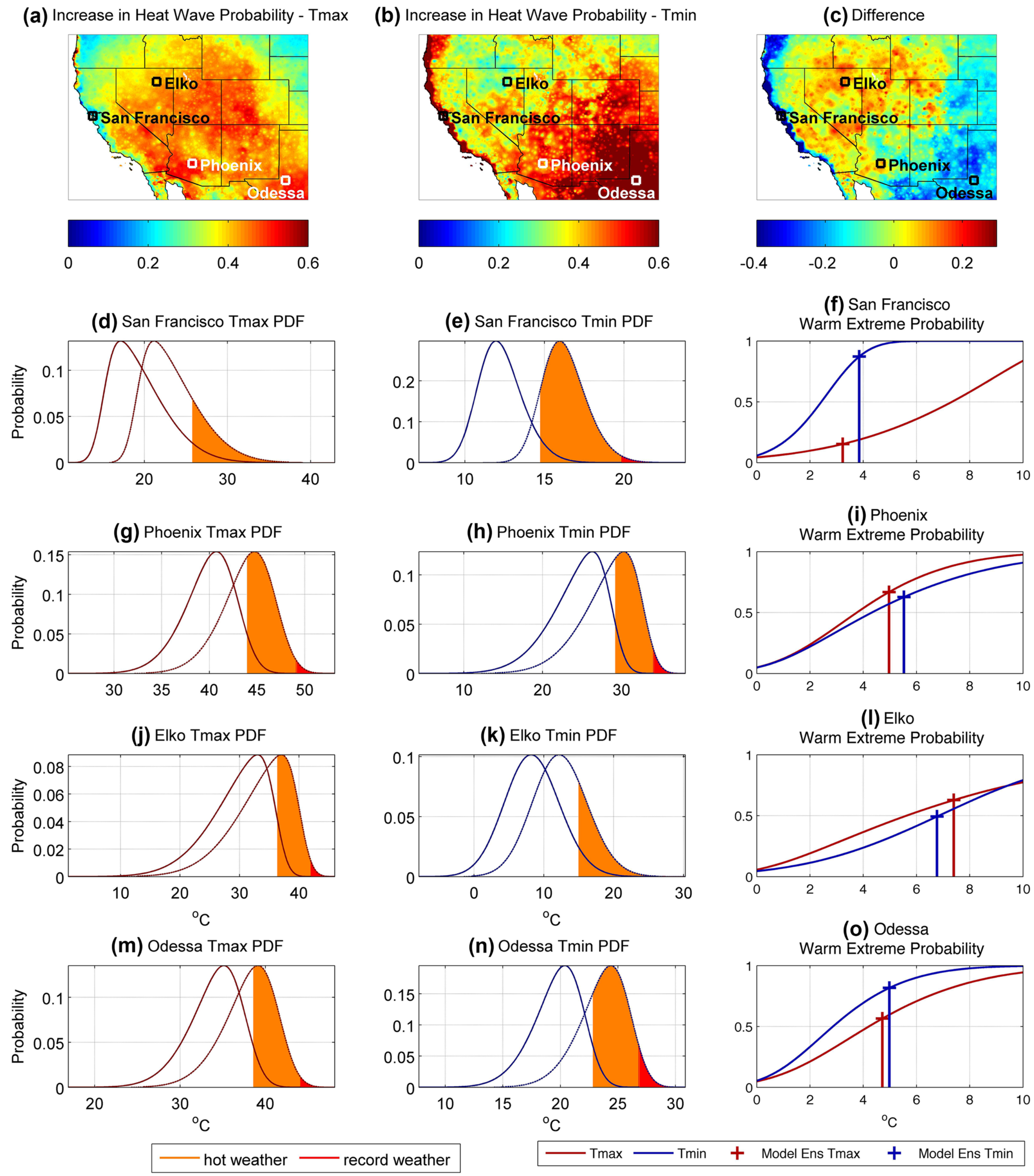

Fig. 3 Heat wave probability resulting from a rigid 4 °C shift in the temperature PDF for **a** Tmax, **b** Tmin, and **c** the difference. Panels **d, g, j, m** and panels **e, h, k, n** show the PDF shift at select cities and the effect on heat wave probability for Tmax and Tmin, respectively. Hot weather represents temperatures above the historical 95th percentile (heat waves) and record weather represents temperatures not previously encountered. Panels (**f, i, l, o**) shows how the warm tails behave as the mode temperature increases. Specifically, the increase in warm extreme probability with incremental increases in mode temperature. *Red and blue lines with cross markers* show the magnitude of the temperature increase projected by the 10-model ensemble by end of century under RCP8.5 for Tmax and Tmin, respectively

the distribution, whereas skew reflects asymmetry more generally (warm and cold tails).

Figure 3d–o illustrate how warm tail length and variance affect extreme probability under a rigid shift. Shifting distributions with shorter warm tails and/or smaller variance results in a higher probability of heat waves than we see for distributions that have long warm tails and/or larger variance, consistent with findings of Ruff and Neelin (2012). A rigid 4 °C warming in Tmax yields heat wave probabilities of 20% in San Francisco and 54% in Phoenix. In contrast, a rigid 4 °C warming in Tmin yields heat wave probabilities of 90% in San Francisco and 46% in Phoenix. This means that, under a rigid shift, in San Francisco it becomes easier to experience a heat wave or break a record for Tmin than for Tmax (Fig. 3d–f). And, for Tmax, it becomes relatively more likely to experience a heat wave or break a record in Phoenix than in San Francisco (Fig. 3d, g). As shown in Figure S2, the Phoenix Tmax distribution has a smaller variance and much shorter warm tails than San Francisco. For Tmin, the San Francisco distribution has slightly longer warm tails than Phoenix, but San Francisco also a much smaller variance, so it is the variance that is primarily responsible for the large change in Tmin HWP at San Francisco. Comparing Elko and Phoenix, we see that Phoenix experiences a larger increase in HWP for both Tmin and Tmax (Fig. 3a, b). From Figure S2 we see that for Tmax, Elko and Phoenix are similar in terms of warm tail length but Phoenix has a much smaller variance. Conversely, for Tmin Elko and Phoenix are similar in variance but Phoenix has much shorter warm tails. In general, locations with a positive value in Fig. 3c experience a faster increase of Tmax heat waves than Tmin heat waves, while negative values indicate a faster increase of Tmin heat waves.

Figure 4 illustrates how warm tails and variance largely determine the rate of increase in HWP. In general, a location having a PDF with long warm tails and high variance will experience the smallest increase in HWP (first quartile) and locations with short warm tails and low variance will see the most dramatic change in HWP (fourth quartile).

While these results illustrate the importance of the historical PDF shape in determining future heat wave probabilities, climate model projections show that the magnitude of future warming will not occur uniformly over the region. Figure 5a, b show the summer temperature increase for Tmax and Tmin, respectively, projected for end of the century according to the RCP8.5 “business as usual” scenario and shown as the average of the ten models. For Tmax the strongest warming is seen in the north (>8 °C) and least amount of warming occurs over California (~5 °C). For Tmin the interior northwest exhibits the most warming

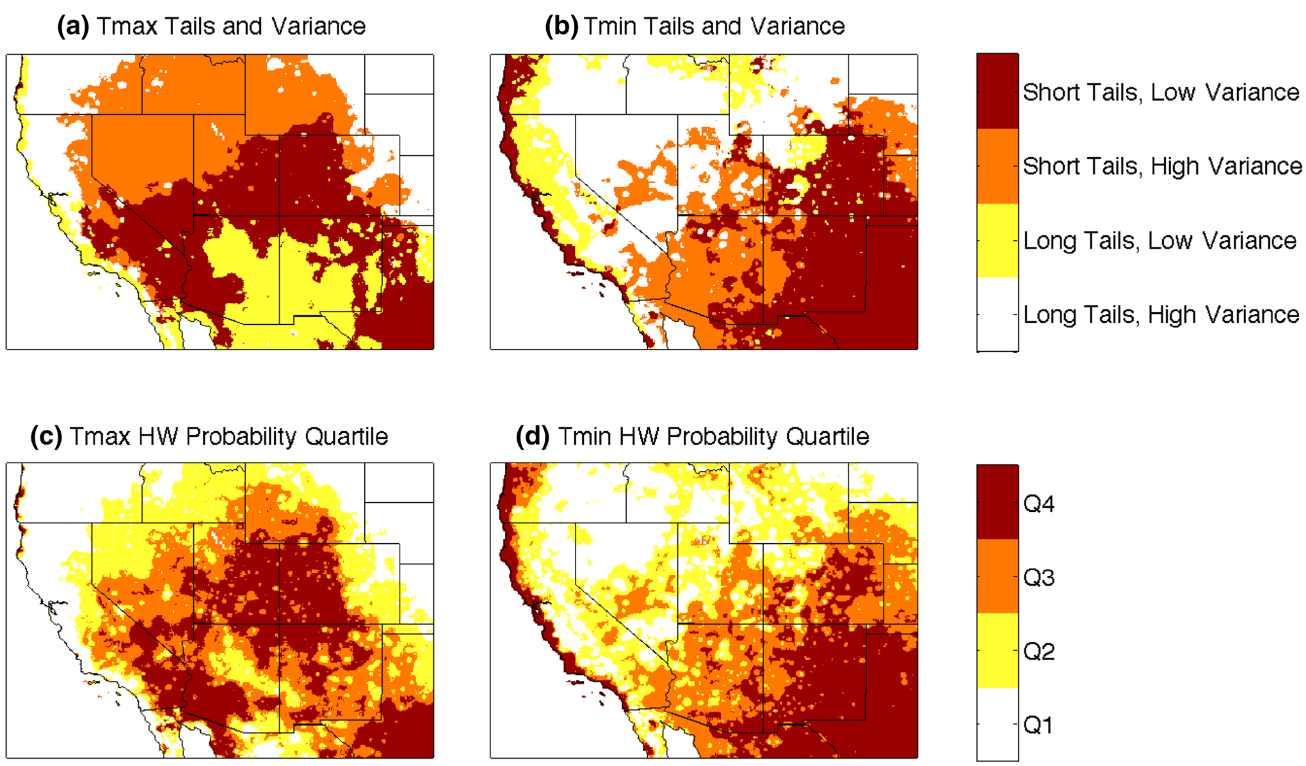

Fig. 4 Illustrates how increases in heat wave probability under a rigid 4 °C shift of the temperature PDF are largely determined by warm tail length and variance. In **a, b** temperature PDFs are classified according to tail length and variance for Tmax and Tmin, respectively. In **c, d** the corresponding heat wave probabilities are ranked by quartiles

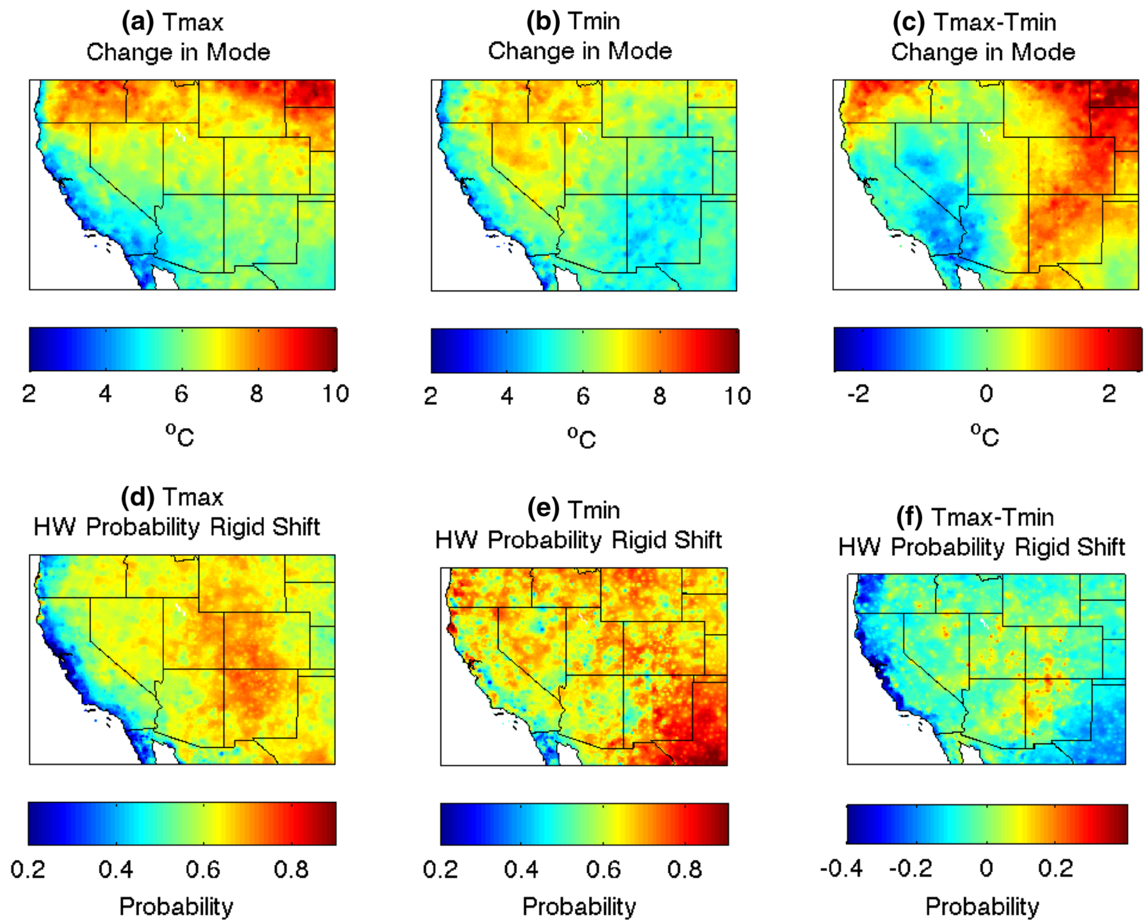

Fig. 5 Summer (JJA) temperature increase by end of century for Tmax (**a**), Tmin (**b**), and the difference (**c**) measured as the change in the mode of the temperature PDF according to the 10-model ensemble. Heat Wave probability by end of century for Tmax (**d**), Tmin (**e**), and the difference (**f**) assuming a rigid shift in the temperature PDF by the amount shown in **a, b**

(~7 °C) with less warming at or near the coast of California and in the southeastern portion of the domain over Texas and New Mexico (~5 °C). Figure 5d, e show the expected HWP that would occur by rigidly shifting the Tmax and Tmin PDFs by the amount predicted by the models in Fig. 5a, b, respectively. The geospatial pattern of heat wave probabilities in this hypothetical exercise is therefore due to the combined effect of (1) the historical PDF shape and specifically variance and warm tail length and (2) local change in mode due to greenhouse gas forcing assuming no change in the shape of the PDF will occur.

For Tmax, a substantial increase in HWP appears in the north (~60–70%) where the magnitude of warming is greatest, however it is buffered somewhat by the long tails/high variance in that region (c.f. Fig. 4 a, c). Although there is comparatively less warming in the 4-corners region, HWP is greater (~80%) due to the short tails/low variance there. So, despite a strong gradient in the magnitude in the mode of climate warming from north to south, HWP does not follow this same pattern. For example, Fig. 3i, l show that Tmax warming is projected to be 7.4 °C at Elko and 5.0 °C at Phoenix, yet heat wave probabilities are projected to be slightly higher at Phoenix (0.63 and 0.67 for Elko and Phoenix, respectively). In California, HWP is much lower due to the combination of less warming there and the effect of long tails/high variance along the immediate coast.

Similarly, for Tmin the pattern of mode temperature change (Fig. 5b) is not reflected in the HWP map (Fig. 5e). This is because in the northwest where warming is stronger, the long tails/high variance of the temperature PDF act to reduce changes in HWP, while in the southeast part of the domain, the short tails/low variance act to enhance HWP. The result is that although there is less warming projected over Texas and New Mexico, there is a dramatic increase in HWP due to the native shape of the temperature PDF.

The differences, Tmax versus Tmin, of the amount of warming and HWP expected are shown in Fig. 5c, f. Here, under a hypothetical rigid shift, differences between Tmax and Tmin in terms of warm extreme probability (Fig. 5f) do not follow differences in warming (Fig. 5c). Over most of the region, excepting California and Nevada, the mode of the Tmax PDF (e.g. average warming) is projected to increase more than Tmin. However, HWP for Tmin increases more than that for Tmax except over the southern deserts around Arizona. Therefore, even under a rigid shift, differences in HWP between Tmax and Tmin can occur due to differences in the native shape of the daily distributions.

6 How projected changes in PDF shape affect future heat wave probabilities

An important area of uncertainty about future climate is how future changes in the shape of the temperature PDF will modify the probability of heat waves. To assess the impact of such shape changes on future HWP, we compare probabilities that would occur under a rigid shift (c.f. Fig. 5d, e) with HWP projected by the models (Fig. 6a, c). A visual comparison of Fig. 5d with Fig. 6a for Tmax and Fig. 5e with Fig. 6c for Tmin suggests the projected increase in HWP can largely be explained by a rigid shift amounting to the change in mode, with some subtle differences explained by future changes in PDF shape. Figure 6b, d show the difference between the projected HWP and the expected HWP based on the rigid shift assumption (i.e. the difference between Figs. 6a and 5d for Tmax and between Figs. 6c and 5e for Tmin). Any difference is therefore due to projected changes in PDF shape and/or scale, which may enhance or offset the effects of background warming.

The effects of changes in PDF shape on future HWP are generally small, contributing +/−10% at most according to the model ensemble HWP. This effect is generally small in comparison to the increase in HWP due to the shifted distribution and is generally within the range of model uncertainty. For example, in Fig. 6f, it is shown that at Point A in New Mexico (Fig. 6d) where we see the strongest positive shape change effect, Tmin HWP would increase by 50% under the shifted mode assumption, but a change in shape increases HWP an additional 9%, yielding a projected probability of 59%. Figure 6e shows visually the PDFs for the projections and the rigid shift assumption at a location selected to maximize this difference, and the difference is slight. In general, there is agreement among models in representing this change in PDF shape, with most models showing enhanced HWP at Point A than we could expect from a rigid shift (Fig. 6f). But this effect is small, especially when we consider the spread among models in representing future HWP (38–72% at Point A). In general, the spread among models in the amount of mode warming is on the order of 1–10 °C, depending on location for both Tmax and Tmin (Fig. S3). Assuming a rigid shift, this spread in mode translates to uncertainty in HWP of 44% (31%) on average over the domain for Tmax (Tmin). Changes in PDF shape can enhance or reduce HWP, so over the domain the average contribution is close to zero. The average absolute contribution over the domain is approximately 4% for both Tmax and Tmin. This is within the range of model uncertainty, and is small relative to the total projected increase in heat wave probability.

Just as for the mode, there is also much uncertainty in the variance and symmetry changes projected for the late twentieth century. Figures S4 and S5 give projected changes in standard deviation and skewness, respectively, for each of the ten models, and Figure S6 shows the agreement among models in terms of the sign of change at each location. From S6, there are some regions where most models (>7 of 10) are in agreement on whether a positive or negative change in variance and/or symmetry occurs. However, uncertainty dominates over most of the domain. For Tmax, models agree on the sign of change in standard deviation (skewness) for only 32% (38%) of the domain. For Tmin, model agreement is slightly better (38 and 58%, respectively for standard deviation and skewness).

7 Summary and discussion

Daily summer temperature probability distributions in the Southwest US are non-Gaussian and asymmetric with shapes that vary considerably across the region. This analysis shows how geospatial differences in the shape of the historical temperature PDF have important implications for future climate change.

The easiest way of envisioning climate change effects on temperature extremes, wherein the entire daily probability distribution shifts uniformly by a given warming amount, is found to capture much of the actual change produced by downscaled climate model simulations. Under a hypothetical rigid shift of the temperature distribution occurring uniformly over the region (i.e. the same amount of warming everywhere), dramatic differences in warm extreme probability would arise geographically due to the effects of variance and warm tail length. Locations with shorter warm tails/smaller variance would see a greater increase in heat wave probability than would long tailed/larger variance distributions under a uniform rigid shift.

In projections, temperature increases due to climate change are not expected to be uniform over continental regions, including the Southwest. An ensemble of 10 downscaled CMIP5 models selected for doing a good job of simulating the region's climate shows important geospatial differences in the amount of warming due to anthropogenic forcing. Greater warming is projected in the northern part of the domain, but future heat wave probability is buffered somewhat by the long warm tails/ high variance of the observed temperature distribution.

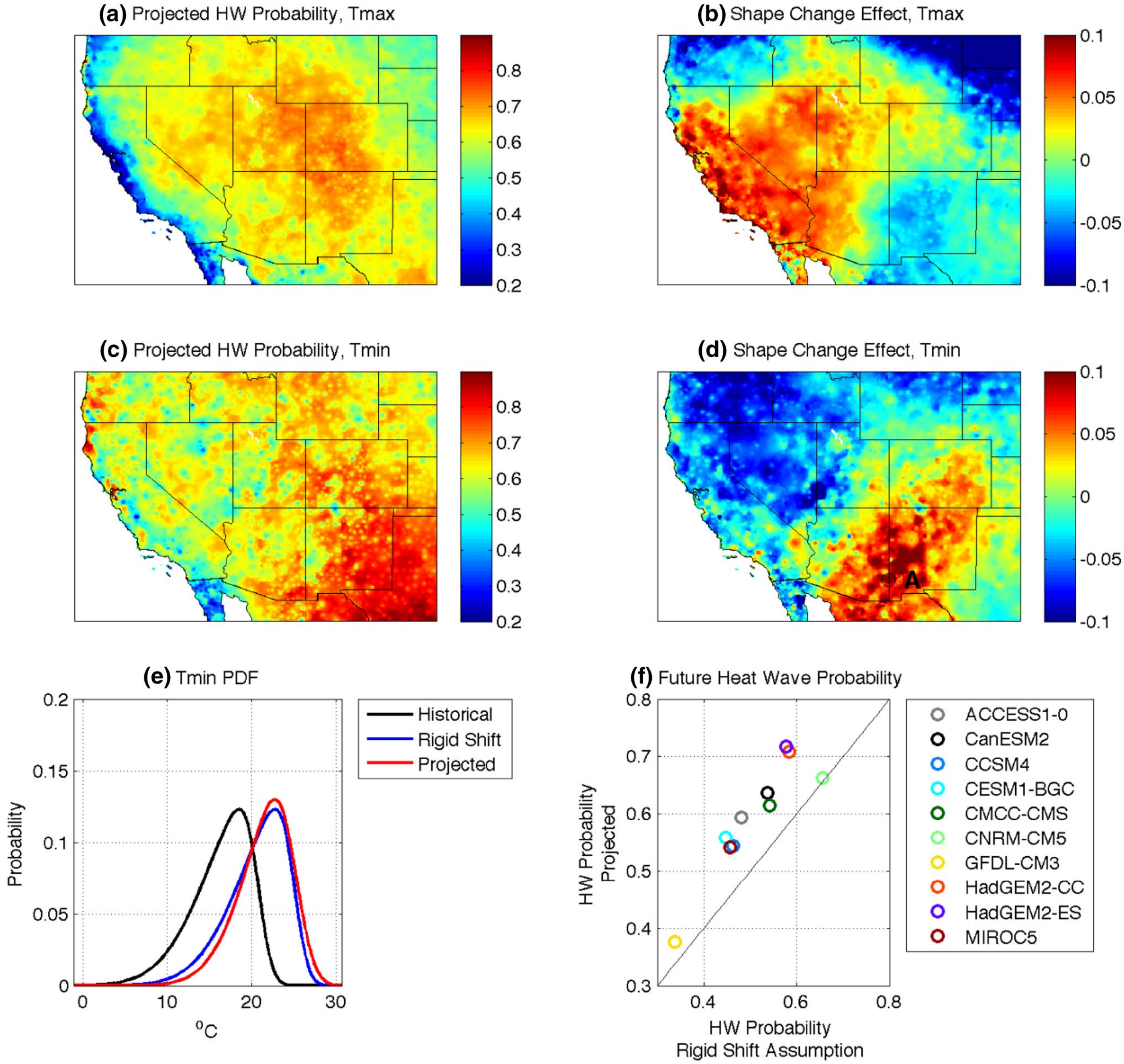

Fig. 6 **a, c** Show the projected heat wave probability for Tmax and Tmin, respectively, calculated directly from daily downscaled model output as the proportion of days exceeding the local historical 95th percentile temperature threshold and shown as the ten model average. **b, d** Show the difference between the projected heat wave probability and what would occur under a rigid shift, and therefore quantifies the contribution due to any PDF shape changes (rigid shift results are shown in Fig. 5**d, e**). **e** Shows the Tmin PDF for "Point A" in New Mexico labeled on the map in **d** for the historical period (*black*), what would occur under a rigid shift (*blue*), and what is projected for the end of century (*red*). **f** Shows the projected HWP for each of the ten CMIP5 models, and what the HWP would be under a rigid shift assumption for Point A in New Mexico

The south exhibits less warming, but heat wave probability is enhanced because temperatures PDFs in that region have a smaller variance and shorter warm tails. In most of the region, average warming is projected to be greater for Tmax than for Tmin by the end of the twentieth century. However, due to differences in the shape of their respective PDFs, heat wave probability is projected to increase more rapidly for Tmin than for Tmax. This asymmetry could have important societal and ecological consequences. Daytime accentuated warming would increase demand for energy and water. Nighttime accentuated warming could detrimentally affect human health during heat waves by limiting the much needed physiological recovery that typically occurs at night.

Increases in heat wave probability projected for the end of the twenty-first century are mostly explained by a rigid shift to warmer temperatures in the daily distributions of Tmax and Tmin. Results presented here suggest only minor influences from modeled changes in PDF shape (variance and skew). While this work aimed to quantify the effect of changes in PDF variance and symmetry on heat wave probability, we found there is much uncertainty among models in the sign and magnitude of these changes.

While all models agree that sizable warming will occur by the end of the twentieth century, there is strong uncertainty in the amount of warming expected. In the southwest we found considerable spread among models in their projections of mode temperature change. For planning purposes, understanding and reducing this first order uncertainty in mean warming is probably more important than quantifying effects of shape changes, at least in the Southwest. For example, uncertainty in the amount of warming projected by end of the century can yield uncertainty in future heat wave probabilities of up to 70% at a location, assuming a rigid shift in the distribution. The added contribution of PDF shape changes may modify heat wave probability slightly, by about +/− 4% on average over the domain.

However, while *changes* in PDF shape may be of lesser importance according to our findings, the historical shape of the temperature distribution is hugely important when it comes to understanding and preparing for future heat waves. Some parts of the Southwest will be relatively more likely to experience warm extremes that are historically rare or unprecedented. Extreme probabilities are also dramatically different for Tmin versus Tmax due to differences in PDF shape. For example, in San Francisco a 4 °C uniform shift results in extreme heat probabilities of 20% for Tmax and 90% for Tmin. Ruff and Neelin (2012) first noted the important importance of tail length for extreme probabilities, which our results support and extend to model projections. While this work focused on heat wave probability in summer, there are implications for cold extremes in winter. For example, a location having a temperature PDF with short cold tails would be expected to see a faster decline in extreme cold events than would a location whose PDF exhibits longer cold tails.

This work employed bias-corrected and downscaled climate model projections where the historical temperature PDFs were corrected to be similar to those observed. This bias-corrected baseline is desirable for comparing changes in PDFs among models. GCMs may not have the spatial resolution needed to resolve some of the finer scale processes responsible for the shape of a location's temperature PDF. For example, marine layer clouds are responsible for the long warm tails of the Tmax distribution along the California coast (Clemesha et al. 2016), but these are not resolved in coarse resolution GCMs. The temperature PDFs represented by GCMs may not be correct due to spatial resolution limitations and/or because resolved processes are not appropriately simulated. For this analysis we focused on ten GCM simulations out of the many available models, so our assessment of inter-model variance is limited. Only one Representative Concentration Pathway (RCP 8.5, the "business as usual" scenario) was analyzed in this work, so our assessment of the likely range of warming is also limited. Given the importance of historical PDF shape in determining future heat wave probabilities, GCMs should be vetted for their ability to represent geospatial differences in realistic PDF tail length and variance. The properties and changes in the distributions have physical meaning in terms of frequencies and intensities of specific weather events contributing to the local climate. Therefore, a model's ability to represent these processes is of utmost importance in understanding and improving model performance and further constraining expectations of future climate change.

Acknowledgements This work was supported by DOI via the Southwest Climate Science Center on a grant titled: "Natural variability in the changing climate: Interaction of interannual, decadal, and century timescales with daily weather", by the National Science Foundation via Grant #F12078-2013-005, and by NOAA via the RISA program through the California and Nevada Applications Program. The observational temperature dataset is freely and publicly available from the University of Washington (ftp://ftp.hydro.washington.edu/pub/blivneh/CONUS/). The LOCA downscaled GCM data are publically available from the USGS Center for Integrated Data Analytics. We thank Mary Tyree for data retrieval and handling. We additionally thank three anonymous reviewers for providing helpful comments during the evaluation of this paper.

References

Azzalini A (2005a) The skew-normal distribution and related multivariate families. Scand J Stat 32:159–188. doi:10.1111/j.1467-9469.2005.00426.x

Azzalini A (2005b) A very brief introduction to the skew-normal distribution. http://azzalini.stat.unipd.it/SN/Intro/. Accessed 11 2016

Azzalini A (2014) The R package 'sn': the skew-normal and skew-t distributions (version 1.1–2). http://azzalini.stat.unipd.it/SN

Azzalini A, Capitanio A (1999) Statistical applications of the multivariate skew normal distribution. J R Stat Soc Ser B 61:579–602. doi:10.1111/1467-9868.00194

California Department of Water Resources (2015) Perspectives and guidance for climate change analysis. California Department of Water Resources (DWR) Climate Change Technical Advisory Group (CCTAG). http://www.water.ca.gov/climatechange/docs/2015/Perspectives_Guidance_Climate_Change_Analysis.pdf. Accessed 11 2016

Cavanaugh NR, Shen SP (2014) Northern hemisphere climatology and trends of statistical moments documented from GHCN-daily surface air temperature station data from 1950 to 2010. J Clim 27:5396–5410

Clemesha RES, Gershunov A, Iacobellis SF, Williams AP, Cayan DR (2016) The northward march of summer low cloudiness along the California coast. Geophys Res Lett 43:1287–1295. doi:10.1002/2015GL067081

Diffenbaugh NS, Pal JS, Giorgi F, Gao X (2007) Heat stress intensification in the Mediterranean climate change hotspot. Geophys Res Lett 34:L11706. doi:10.1029/2007GL030000

Gershunov A, Guirguis K (2012) California heat waves in the present and future. Geophys Res Lett. doi:10.1029/2012GL05297

Guirguis K, Gershunov A, Tardy A, Basu R (2014) The impact of recent heat waves on human health in California. J Appl Meteorol Clim 53:3–19

Guirguis K, Gershunov A, Cayan DR (2015) Interannual variability in associations between seasonal climate, weather, and extremes: wintertime temperature over the Southwestern United States. Environ Res Lett. doi:10.1088/1748-9326/10/12/124023

Hidalgo HG, Dettinger MD, Cyan DR (2008) Downscaling with constructed analogues: daily precipitation and temperature fields over the United States. California Energy Commission report CEC-500-2007-123, pp 82

IPCC (2012) Managing the risks of extreme events and disasters to advance climate change adaptation. A special report of working groups I and II of the intergovernmental panel on climate change. In: Field CB, Barros V, Stocker TF, Qin D, Dokken DJ, Ebi KL, Mastrandrea MD, Mach KJ, Plattner GK, Allen SK, Tignor M, Midgley PM (eds) Cambridge University Press, Cambridge

Kodra E, Ganguly AR (2014) Asymmetry of projected increases in extreme temperature distributions. Sci Rep 4:5884. doi:10.1038/srep05884

Li H, Sheffield J, Wood EF (2010) Bias correction of monthly precipitation and temperature fields from intergovernmental panel on climate change AR4 models using equidistant quantile matching. J Geophys Res 115:D10101. doi:10.1029/2009JD012882

Livneh B, Rosenberg EA, Lin C, Nijssen B, Mishra V, Andreadis KM, Maurer EP, Lettenmaier DP (2013) A long-term hydrologically based dataset of land surface fluxes and states for the conterminous United States: update and extensions. J Clim 26:9384–9392

Loikith PC, Lintner BR, Kim J, Lee H, Neelin JD, Waliser DE (2013) Classifying reanalysis surface temperature probability density functions (PDFs) over North America with cluster analysis. Geophys Res Lett 40:3710–3714. doi:10.1002/grl.50688

Maurer EP, Wood AW, Adam JC, Lettenmaier DP, Nijssen B (2002) A long-term hydrologically-based data set of land surface fluxes and states for the conterminous United States. J Clim 15:3237–3251

National Climatic Date Center (2009) Data documentation for data set 3200 (DSI-3200): surface land daily cooperative summary of the day, report, Asheville, NC. http://www1.ncdc.noaa.gov/pub/data/documentlibrary/tddoc/td3200.pdf. Accessed 11 2016

Perron M, Sura P (2013) Climatology of non-Gaussian atmospheric statistics. J Clim 26:1063–1083. doi:10.1175/JCLI-D-11-00504.1

Pierce DW, Cayan DR, Thrasher BL (2014) Statistical downscaling using localized constructed analogs (LOCA). J Hydrometeorol 15(6):2558–2585

Pierce DW, Cayan DR, Maurer EP, Abatzoglou JT, Hegewisch KC (2015) Improved bias correction techniquesx for hydrological simulations of climate change. J Hydrometeorol 16:2421–2442. doi:10.1175/JHM-D-14-0236.1

Poumadère M, Mays C, Le Mer S, Blong R (2005) The 2003 heat wave in France: dangerous climate change here and now. Risk Anal 25:1483–1494. doi:10.1111/j.1539-6924.2005.00694.x

Ruff TW, Neelin JD (2012) Long tails in regional surface temperature probability distributions with implications for extremes under global warming. Geophys Res Lett 39:L04704. doi:10.1029/2011GL050610

Schär C, Vidale PL, Lüthi D, Frei C, Häberli C, Liniger MA, Appenzeller C (2004) The role of increasing temperature variability for European summer heat waves. Nature 427:332–336

Sillmann J, Kharin VV, Zhang X, Zwiers FW, Bronaugh D (2013) Climate extremes indices in the CMIP5 multimodel ensemble: Part 1. Model evaluation in the present climate. J Geophys Res Atmos 118:1716–1733. doi:10.1002/jgrd.50203

Simolo C, Brunetti M, Maugeri M, Nanni T, Speranza A (2010) Understanding climate change-induced variations in daily temperature distributions over Italy. J Geophys Res 115:D22110. doi:10.1029/2010JD014088

Simolo C, Brunetti M, Maugeri M, Nanni T (2011) Evolution of extreme temperatures in a warming climate. Geophys Res Lett 38:L16701. doi:10.1029/2011GL048437

Stefanova L, Sura P, Griffin M (2013) Quantifying the non-Gaussianity of wintertime daily maximum and minimum temperatures in the southeast. J Clim 26(3):838–850

Taylor KE, Stouffer RJ, Meehl GA (2012) An overview of CMIP5 and the experiment design. Bull Am Meteorol Soc 93(4):485–498

Van den Dool HM (1994) Searching for analogues, how long must we wait? Tellus A 46(3):314–324

Weaver SJ, Kumar A, Chen M (2014) Recent increases in extreme temperature occurrence over land. Geophys Res Lett 41:4669–4675. doi:10.1002/2014GL060300

Zhang X, Alexander L, Hegerl GC, Jones P, Tank AK, Peterson TC, Trewin B, Zwiers FW (2011) Indices for monitoring changes in extremes based on daily temperature and precipitation data. WIREs Clim Chang 2:851–870. doi:10.1002/wcc.147